Velocities in the Analysis of cGPS Data from Volcanoes, Somma-Vesuvius Volcano, Italy.

F. Alejandro Nava Pichardo [1], Lenin Ávila-Barrientos [1,2], Carlos E. Reinoza [1]

[1] Centro de Investigación Científica y de Educación Superior de Ensenada, Baja California. División de Ciencias de la Tierra, Departamento de Sismología. Carretera Ensenada – Tijuana No. 3918, Zona Playitas, 22860, Ensenada, Baja California, México. ORCID: 0000-0001-6778-2017 (FANP), 0000-0003-2347-3161 (CER)

[2] Dirección Adjunta de Investigación Humanística y Científica, CONAHCYT, Av. Insurgentes Sur 1582, Col. Crédito Constructor, Alcaldía Benito Juárez, C. P. 03940, Ciudad de México. ORCID: 0000-0001-7451-8636 (LA-B)

Corresponding author: Lenin Ávila-Barrientos, lenavila@cicese.mx

Abstract

GPS/GNSS monitoring of surface deformation in volcanoes is a valuable tool for studying ongoing magmatic processes on active volcanoes, but displacements measured at different sites do not have a common reference level related to a known deformation status of the volcanic edifice. Velocities do not have this disadvantage, since they all have a well-defined reference zero level, so that positive or negative velocities measured on a given station component mean that the station is moving towards or away from the direction of the components, respectively. We propose that velocities, obtained directly from cGPS displacement measurements, may be useful to interpret different aspects of the observed

volcano deformations, and we present five tools that can be useful in visualizing and comparing measurements at different stations. The proposed technique and tools are illustrated by applying them to a public and complete dataset of continuous GPS time series of the Somma-Vesuvius Volcano, Italy.

Keywords: GPS volcano monitoring, Somma-Vesuvius volcano, velocities, Volcanic hazard.

Introduction

Whether obtained exclusively from the Global Positioning System (GPS) or incorporating other constellations of the Global Navigation Satellite System (GNSS), the continuous GPS/GNSS (cGPS/cGNSS) observations are an important tool for monitoring of volcanoes and early warning systems (Dixon *et al.* 1997; Lowry *et al.* 2001; Bartel *et al.* 2003; Janssen *et al.* 2002; Cabral-Cano *et al.* 2008; Moran *et al.* 2008; Lee *et al.* 2015; Larson *et al.* 2010; Savage *et al.* 2010; Ávila-Barrientos *et al.* 2021). These observations are used to characterize the activity associated with volcanoes, and the cGNSS data analyses show a correlation between surface deformation and magma migration (Mogi 1958; Nishimura *et al.* 2001; Mann *et al.* 2002; Miyagi *et al.* 2004; Fournier *et al.* 2009; Hotta *et al.* 2019). Continuous observations of ground deformation can contribute to reduce volcanic risk, particularly for volcanoes sited near populated areas (Tilling 2008).

Signals originating in the volcanic upper conduit, which may include seismicity and ground deformation at different scales, can be used as an indicator of eruptive activity in volcanoes due to increasing pressure in magma reservoirs (Chaussard *et al.* 2013, Ghosh *et al.* 2021). Ground deformation changes of the volcanic edifice precede the eruptions by times that range from hours to months (Lee *et al.* 2015; Janssen 2007), and these changes could be applicable for timely evacuation (Salzer *et al.* 2014).

The results of cGNSS monitoring at various sites, or stations, located on or near a volcanic edifice, are time series corresponding to the three components of position, usually referred to as displacement, at each site, and the values of each of these series are measured with respect to reference values that, in general, vary from one site to another, and that have no relation to a given state of deformation of the volcanic edifice, since it is impossible to know exactly what is the state of repose of a given volcano.

To correctly interpret the information from cGNSS monitoring, it is necessary to be able to compare the observations obtained at different stations; and many studies do qualitative comparisons but, without a common reference level, quantitative comparison is not possible. Here, We present a set of tools for visualizing and comparing measurements at different stations applied to a public dataset of continuous GPS time series of the Somma-Vesuvius Volcano, Italy.

The Somma-Vesuvius Volcano data

Each feature of the approach we propose will be illustrated by application to the Somma-Vesuvius Volcano data set of cGPS displacements used by De Martino *et al.* (2021), who kindly made the data freely accessible. De Martino *et al.* (2021) present an introduction to the volcano itself and to the data set. Here, we will review only some aspects of the post-processing of the displacement time series and concentrate on the application of the velocity approach to gather information about the volcanic processes.

Nine cGPS stations monitor the activity of the Somma-Vesuvius Volcano (Table 1 and Fig. 1), for details on the instrumentation the reader is referred to De Martino *et al.* (2021) and references therein.

Table 1 cGPS stations located on the Somma-Vesuvius Volcano.

Station	Longitude (°)	Latitude (°)	Elevation (km)
AGR1	14.343	40.811	0.070
BKE1	14.439	40.819	0.864
BKNO	14.430	40.830	0.959
ONPI	14.411	40.779	0.123
OSVE	14.397	40.828	0.624
PRET	14.477	40.849	0.209
SANA	14.412	40.869	0.156
TERZ	14.475	40.808	0.180
VOLL	14.348	40.883	0.033

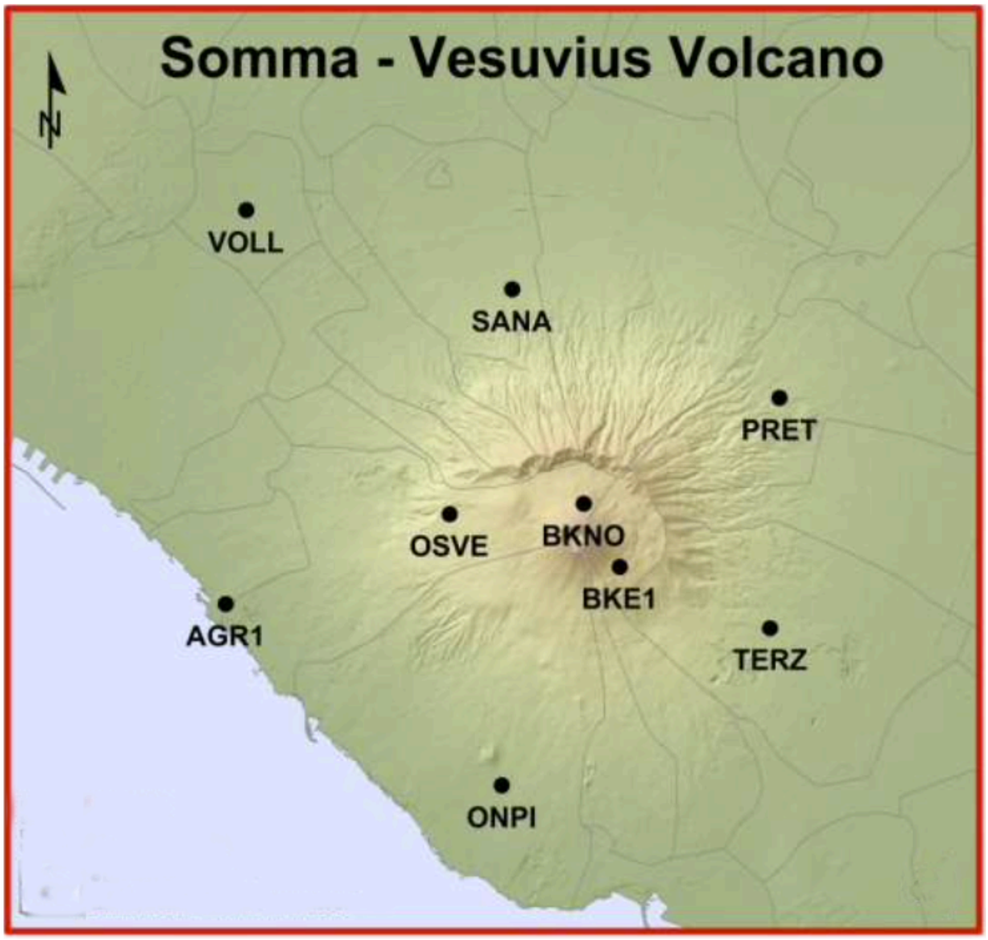

Fig. 1 cGPS stations located on the Somma-Vesuvius Volcano (modified from De Martino *et al.* (2021).

The original final daily position time series are shown in Fig. 2, where time is expressed in modified Julian days (De Martino *et al.* 2021). The series show strong high-frequency noise that obscures the intermediate- and long-period behavior, and they have gaps, i.e. missing data. Since we need equispaced data, interpolation is necessary, but large gaps cannot be interpolated without introducing unwarranted information, so we will use only segments having gaps ≤ 3 data.

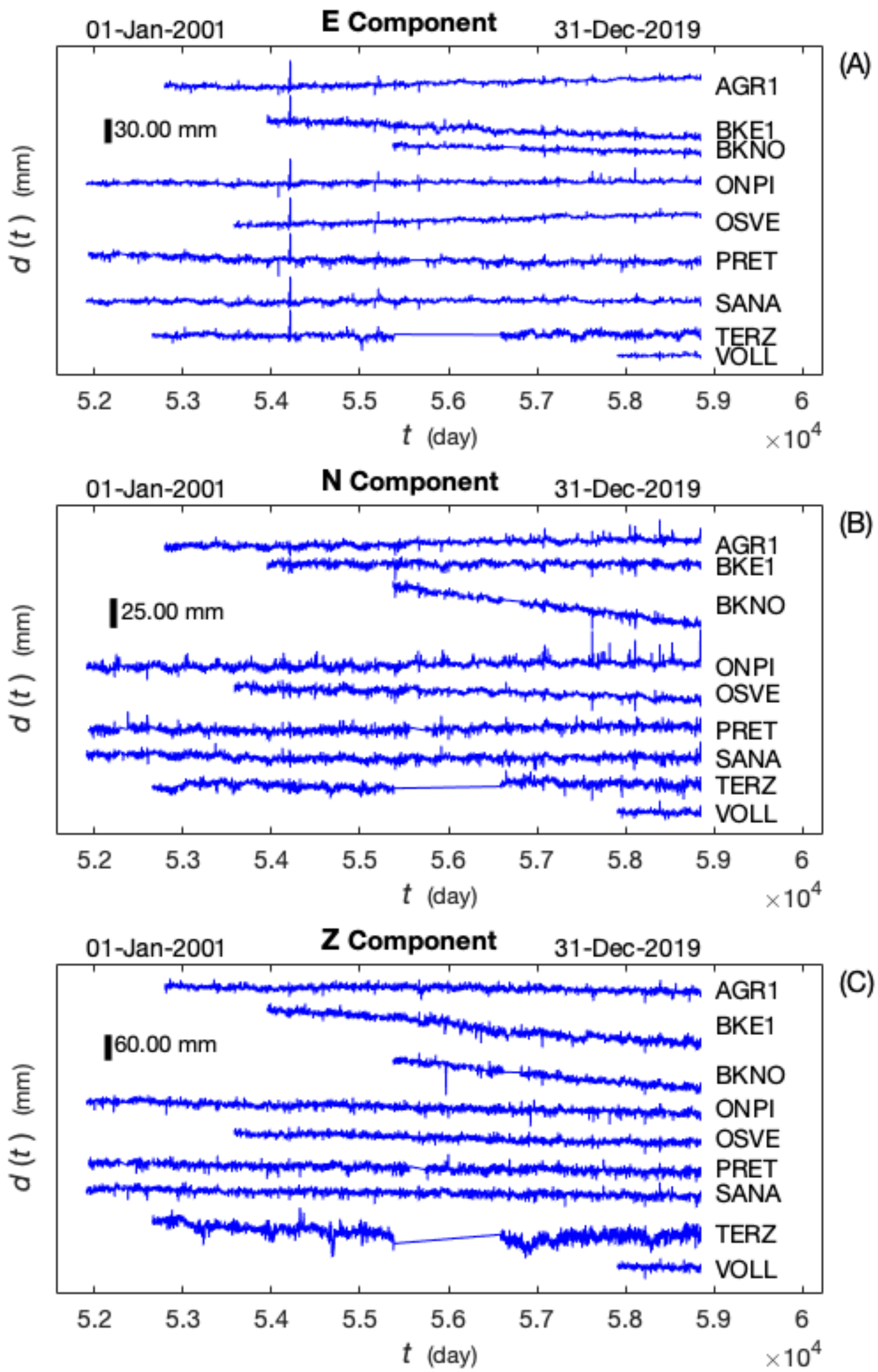

Fig. 2 Original final daily position displacement time series obtained from De Martino *et al.* (2021) E-W component (A), Nort-South component (B), and Z or U component (C).

We tried several interpolation techniques by randomly creating gaps in a long series, interpolating the missing values, and comparing the spectrum of the reconstituted series with that of the original one. We found, surprisingly, that the interpolation that caused the smallest changes in the spectrum was linear interpolation, so this was the interpolation method used for the series shown below.

Figure 3 is an example of the interpolation and segmentation process for two stations. The original series are shown in (A) and (C), where circles indicate interpolated values. Since long-period features in the series show durations of about 100 samples and since the filtering we will need (discussed below) introduces tails about 70 samples long, we will only keep segments larger than 300 samples. These segments, identified by their occurrence order, are the ones used for further processing.

Since the displacement series have large high-frequency noise and since we will be using velocities derived from the displacement time series and differentiation enhances the high frequencies, it was necessary to low-pass the signals; we did this by means of a Butterworth filter (Hamming 1977) with reference frequency $f_c = 0.01$ day^{-1} and filter order $\mathrm{N_B} = 6$. Other filter settings were tried, but we found that the above mentioned settings were the ones which gave sufficiently good results without over-filtering.

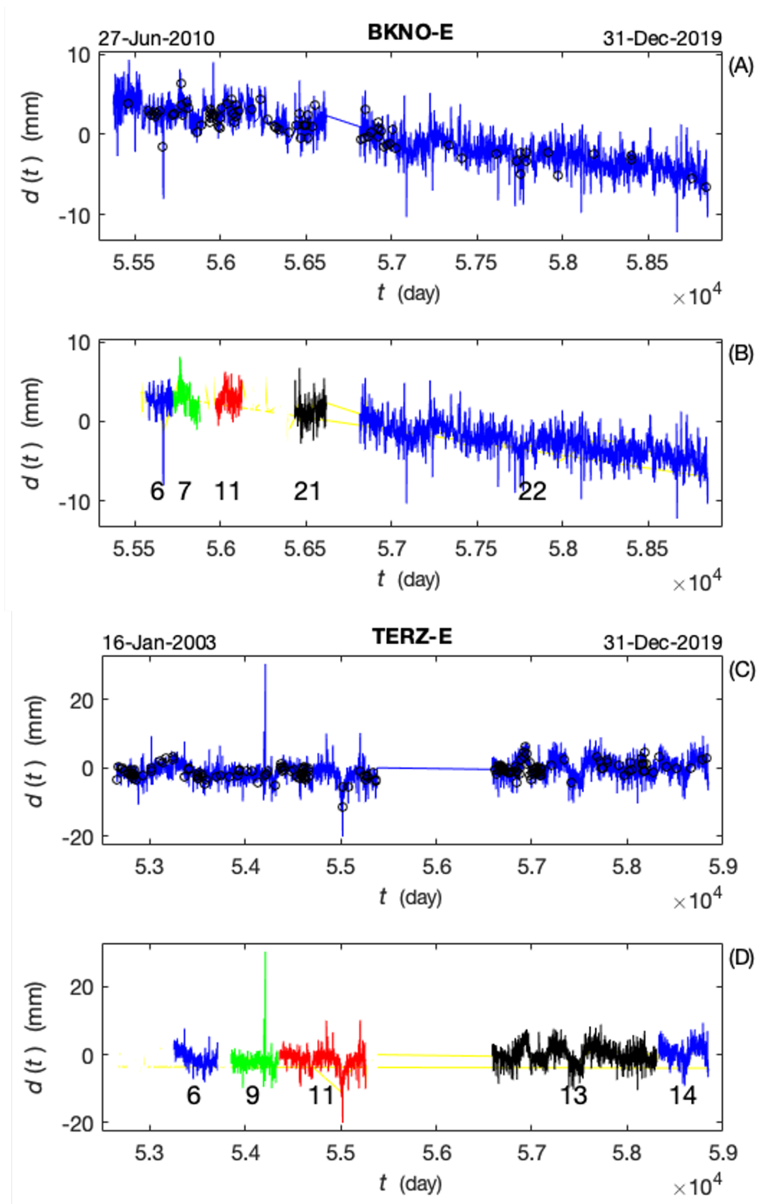

Fig. 3 Example of the interpolation and segmentation process. (A) shows the original series BKNO-E (East-West component), and the circles indicate the interpolated values, and (B) shows the continuous series that are saved for further use. (C) and (D) are the corresponding series for TERZ-E.

Figure 4 shows an example of the low-pass filtering of the displacement time series: the original (equispaced) series is shown in (A), and its Fourier amplitude spectrum is shown in (B). The filtered series is shown in (C) as a thick red line over the original time series (light blue), and its amplitude spectrum is shown in (D).

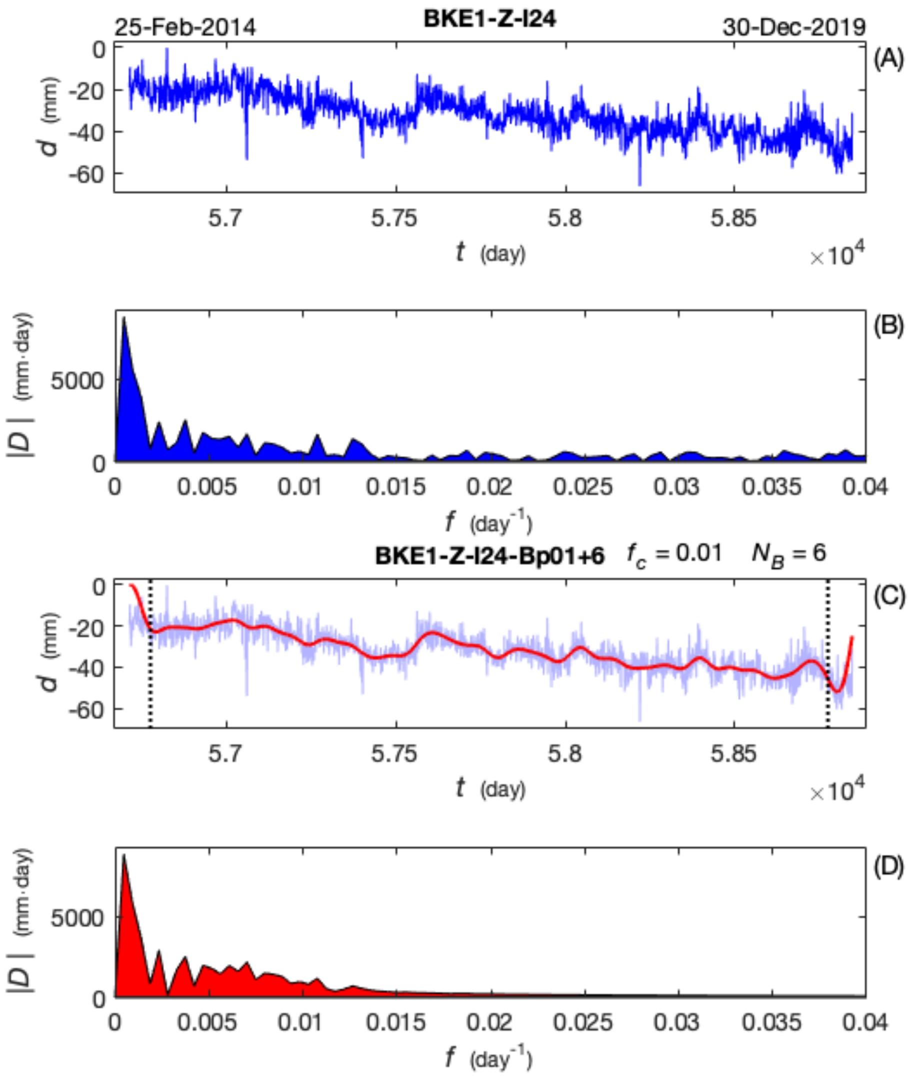

Fig. 4 Example of filtering. Original interpolated segment (A) and its Fourier amplitude spectrum (B); the filtered series is shown in (C) as a thick red line over the original in light blue, and its spectrum in (D). The dotted vertical lines in (C) indicate the tails from the filtering to be discarded.

Velocities

Once the high-frequency noise has been filtered out from the displacement series, the task of interpretation begins, but interpretation is complicated by the fact that the displacements constituting the time series do not have a common reference level, each series is referred to some zero value, different for each station, that is completely arbitrary with respect to the state of expansion or contraction in the volcanic edifice. It is impossible to know the displacement value that corresponds to a "repose" state, i.e. neither expansion nor contraction, of the volcano.

Hence, we take resort to displacement velocities

$$v_i = (d_i - d_{i-1})/\Delta t \,, \quad (1)$$

where d_i is the i'th element of the displacement series and Δt is the sampling interval. Velocities have a well-defined zero level, and positive or negative velocities for a given component of a station indicate unequivocally that the station is moving in the positive or negative direction of that component, respectively, so periods of motion towards a given direction are easy to recognize and evaluate. Also, since zero levels are well defined, it is possible to construct 3D vectors that correspond to the total velocity at a given time for some station, which totally characterize how the station is moving in terms of total velocity magnitude (or amplitude), azimuth, and elevation.

Figure 5 shows an example of a filtered displacement time series (A), where a reference zero level has been purposefully omitted, and the corresponding velocity time series (B), where positive and negative episodes have been assigned different shadings to make them easier to distinguish. The vertical dotted lines show how the zero velocity values correspond to the extrema of the displacement. This figure clearly illustrates the increase in frequency where one simple displacement excursion, such as the one going from A to B (displacement goes simply up and down) corresponds to two velocity episodes, one positive and one negative. A second, slightly more complicated, displacement excursion, going down from C and coming back up at D, results in four velocity episodes, due to small details in the displacement. Thus, since derivation is a high-pass filter, velocities show higher frequencies and more details than the corresponding displacements.

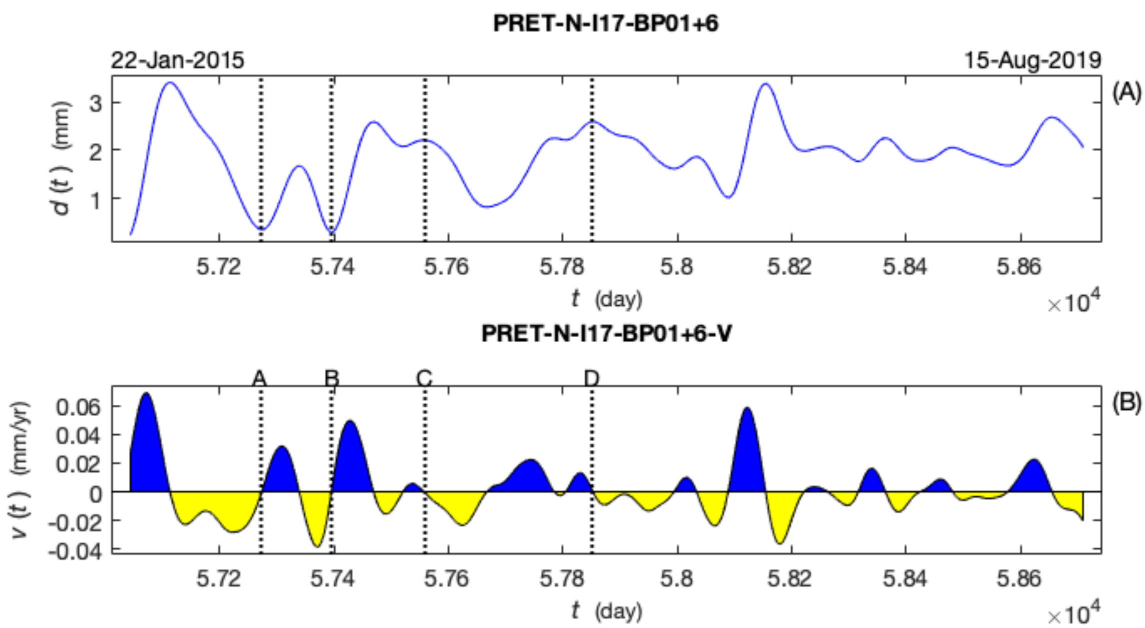

Fig. 5 Example of a filtered displacement time series (A) and the corresponding velocity time series (B), where positive (blue) and negative (yellow) velocity episodes are shown with different shadings to make them easier to distinguish. Vertical dotted lines with labels indicate features discussed in the text.

Interstation Velocity Differences

Once the velocity time series have been obtained, it is useful to compare velocity records from different stations, because the differences in velocity amplitudes and times may yield valuable information about the deformation source. The most immediate way is to choose segments of velocity time series sampled over the same period at different stations, let them be denoted by v_1 and v_2, and plot them together in one or in adjacent figures, but many times it is difficult to see how differences at some time relate to those at other times. Another straightforward way is to plot the difference $v_1 - v_2$, but this is an ambiguous plot because the same value can be obtained from an infinite number of combinations of different values.

Here, we propose a way to present the data that, while not extracting additional information, makes the available information more accessible and easier to see and interpret. This method is shown in Fig. 6, which shows the series to be compared in panel (A), where v_1 is the vertical component from station BKE1, and panel (B), where v_2 the vertical component from station BKNO, and their difference is plotted in panel (D). Panel (C) shows both series, but the differences between them have been shaded in two colors: blue indicates $|v_1| > |v_2|$ and orange corresponds to $|v_2| > |v_1|$, i.e. the colors identify which signal is dominant at the time. The resulting figure looks like a colored ribbon, where the width of the ribbon indicates the magnitude of the differences, and the upper and lower limits of the ribbon, together with the color, show at a glance both the sign and the amplitude of each component. This ribbon helps to interpret correctly the difference shown in panel (D), which, in turn, shows the numeric value of the difference corresponding to the ribbon's width.

It is possible to pick times, and optionally label them, to indicate features that help to understand the results. For instance, in Fig. 6, the time indicated by a vertical dashed line labeled c, corresponds to the maximum difference, chosen in panel (D) and corresponds to the maximum ribbon width in panel (C), when v_2 had the largest (positive) amplitude (red) and v_1 had a small amplitude that being negative contributed to the large difference. At time a, the width of the ribbon is almost zero (the difference between the signals is zero), as shown in (D), but the height of the ribbon tells that the signals themselves are not zero, both are negative and the amplitude of v_1 is larger than that of v_2 just before time a, and smaller just after it. At time b, the ribbon is wide because v_1 is large, while v_2 is small. Finally, at time d, the difference is again zero, but both signals are positive.

A feature symmetric with respect to zero, would indicate stations moving in the same manner but in opposite directions for the observed component. For every chosen time, the relevant values can be printed for later use.

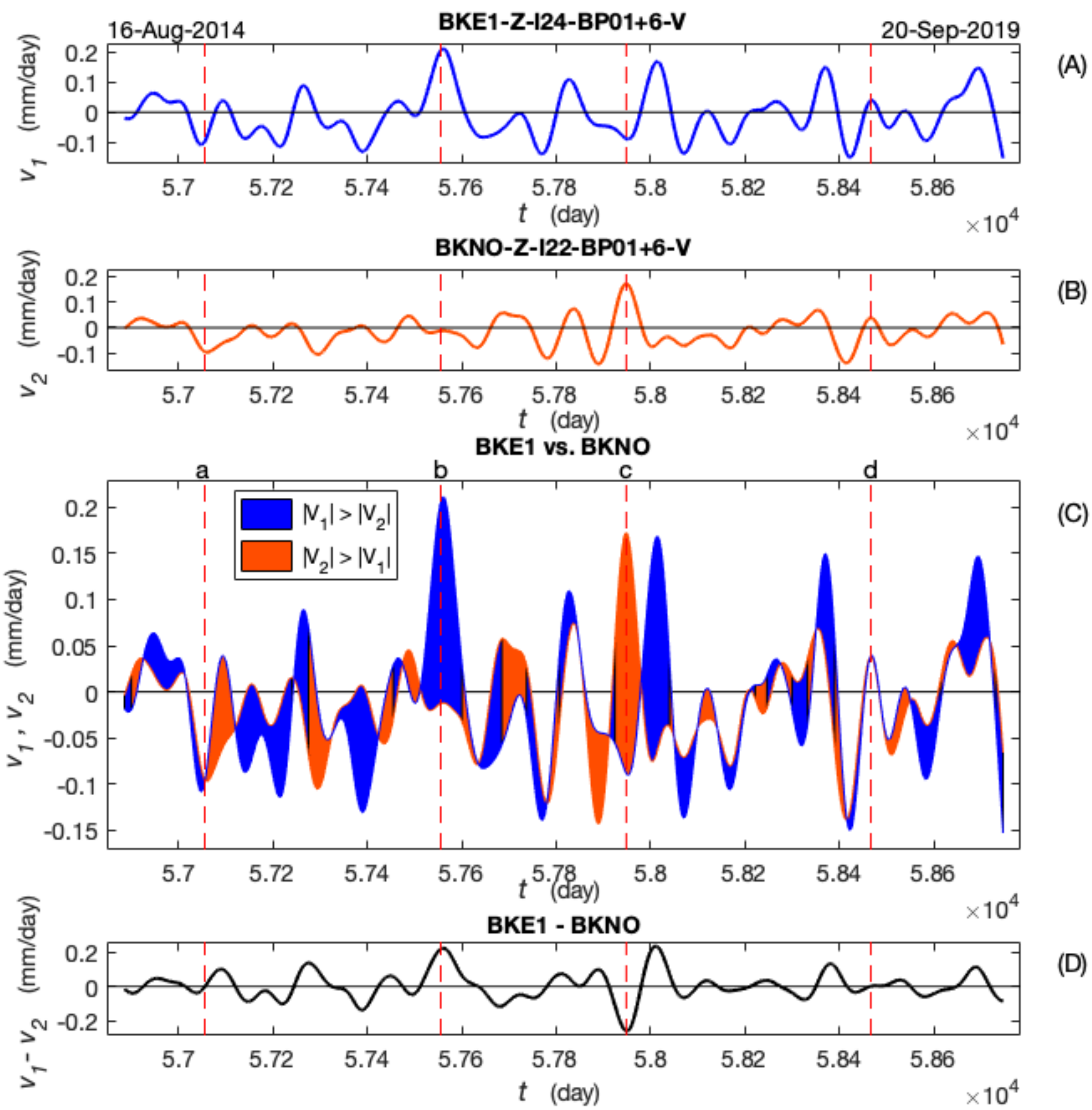

Fig. 6 Temporary comparison of velocity time series between A) BKE1 and B) BKNO stations for the vertical component. D) Difference between the signals, $v_1 - v_2$. C) Both signals, with shading between them colored according to which signal has the largest absolute value.

Co-velocities

The second comparison between two stations is whether both stations are moving in the same or in opposite directions, evaluated by what we call *co-velocities* defined as

$$w = \sqrt{v_1 v_2}\ \operatorname{sgn} v_1 = w^{=} + i w^{\neq},$$

so that *w* is proportional to the product of the velocities and has units of velocity, it is real and equal to $w^{=}$ when both velocities have the same sign, and imaginary and equal to $iw^{\neq}$ when they have different signs, and is positive or negative according to the sign of v_1; if one or both velocities are zero, then $w = 0$ because the question of whether both stations are moving in the same direction is meaningless.

An example of this comparison is shown in Fig. 7, where the velocity series to be compared, the N-S components at BKE1 and TERZ, are shown in panels (A) and (B), $w^{=}$ is shown in panel (C), where episodes when both stations were moving North are blue-shaded and when both were moving South are yellow-shaded. Panel (D) shows $w^{\neq}$ episodes when the first station was moving North while the second station was moving South (blue-shaded) or vice-versa (yellow-shaded). Letters in the extreme left of each plot indicated the direction of motion; for panels (C) and (D) the first letter corresponds to the first station and the second letter to the second station.

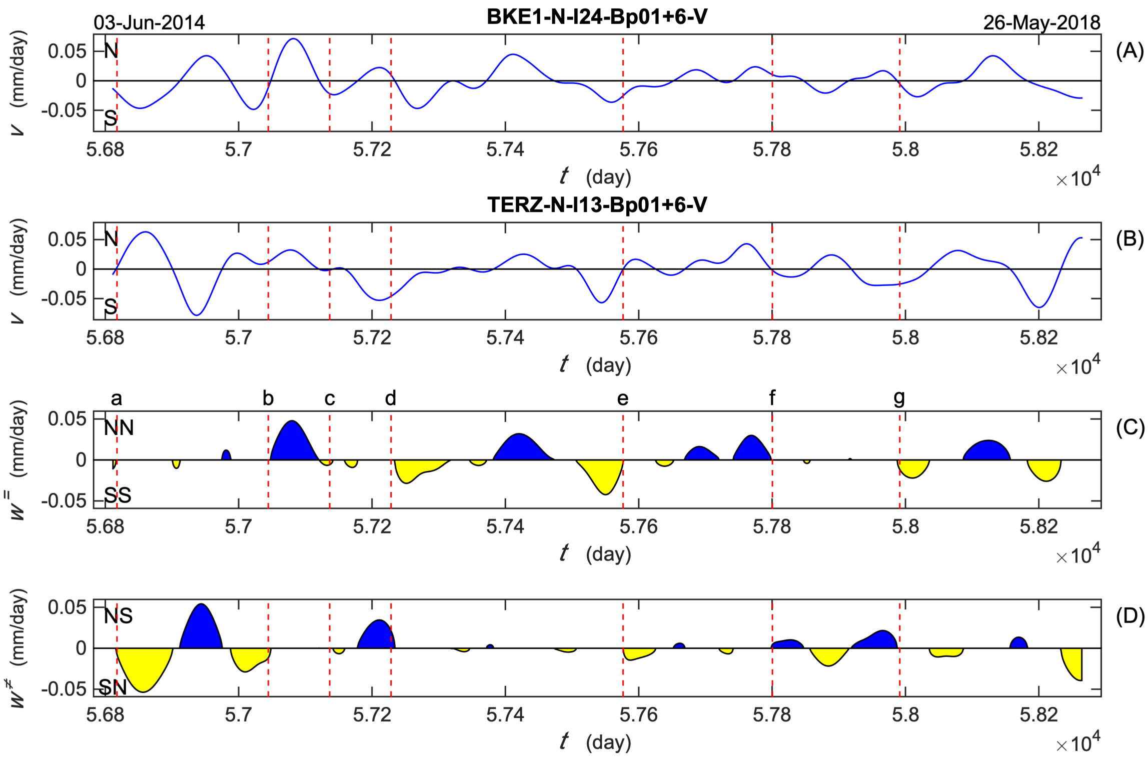

Fig. 7 Co-velocities for comparison of the N-S velocity components shown in (A) and (B), (C) shows $w^{=}$ and (D) shows $w^{\neq}$.

A large episode of motion in opposite directions, starting at time a with BKE1 moving South and TERZ moving North, then reversing directions, then reversing directions again and ending at time b. This episode was followed by one with both stations moving in the same direction between times b and c, followed by another with opposite directions between times c and d, and another long episode of mainly same direction between times d and e. Another episode with (mostly) opposite directions occurs between times f and g.

Longitudinal and Transverse

The horizontal velocity components at two stations can be compared in the same way, but their interpretation in terms of a possible source is not forthwith, because the location of the source is unknown. Hence, as a third tool for easier interpretation, we propose rotating the horizontal components to obtain components along the azimuth from the southernmost station, henceforth referred to as station 1, to the northernmost one, station 2, which we will call the longitudinal L, and components perpendicular to the azimuth direction, which we will call transverse T. When the azimuth equals 90°, L coincides with E-W, and T with N-S. These components, illustrated in Fig. 8, make interpretation more straightforward, particularly the longitudinal one, because velocities with different signs mean that stations are getting farther from or nearer to each other.

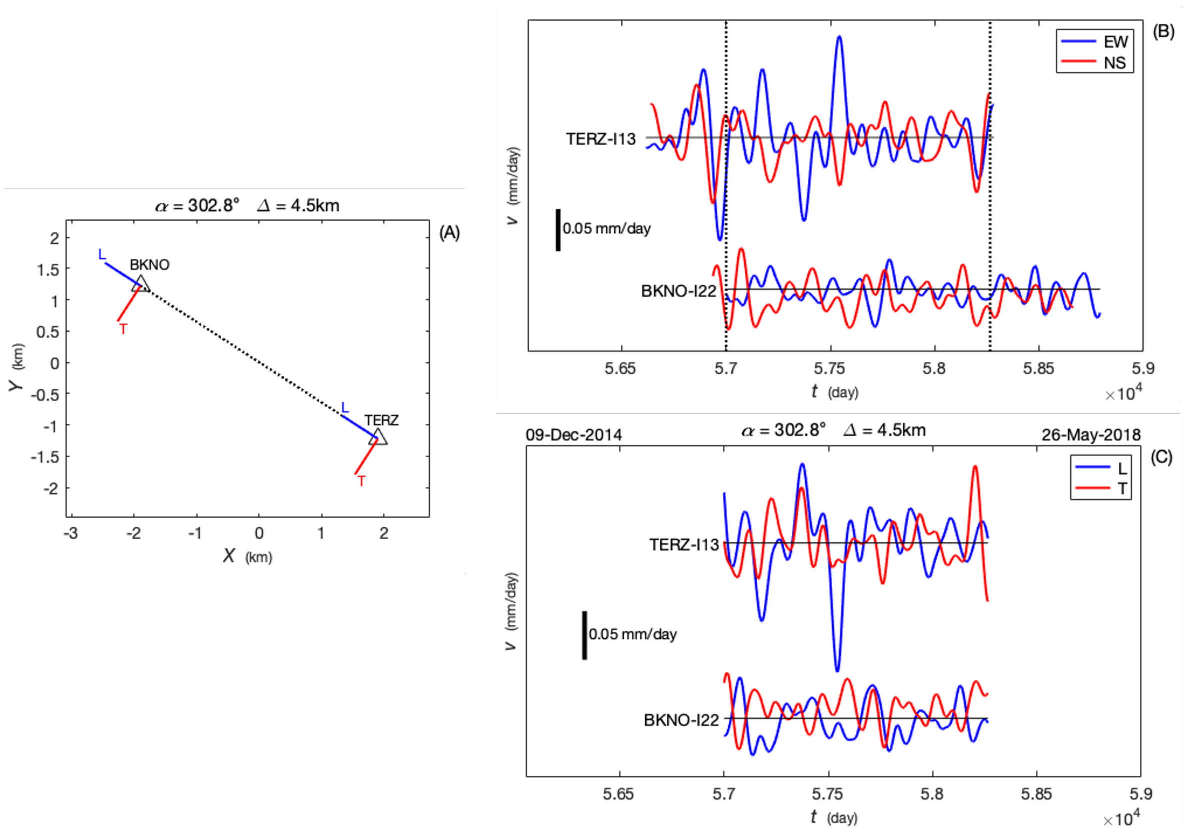

Fig. 8 Longitudinal and transverse velocity components for two stations, in (A) α is the azimuth from station 1 (the southernmost one, TERZ) to station 2 (BKNO) and Δ is the distance between them; longitudinal components are represented as blue lines, and transverse components as red lines. Panel B shows the E-W (blue) and N-S (red) components for both

stations; vertical dotted lines indicate the interval common to both stations. Panel C shows the rotated longitudinal (blue) and transverse (red) components.

This comparison is particularly easy to make using co-velocities as shown in Fig. 9, which shows that stations are moving mainly in the same direction until $t = 57758$ days (red vertical dotted line labeled a), indicated on the figure by a, and mainly in opposite directions from then on.

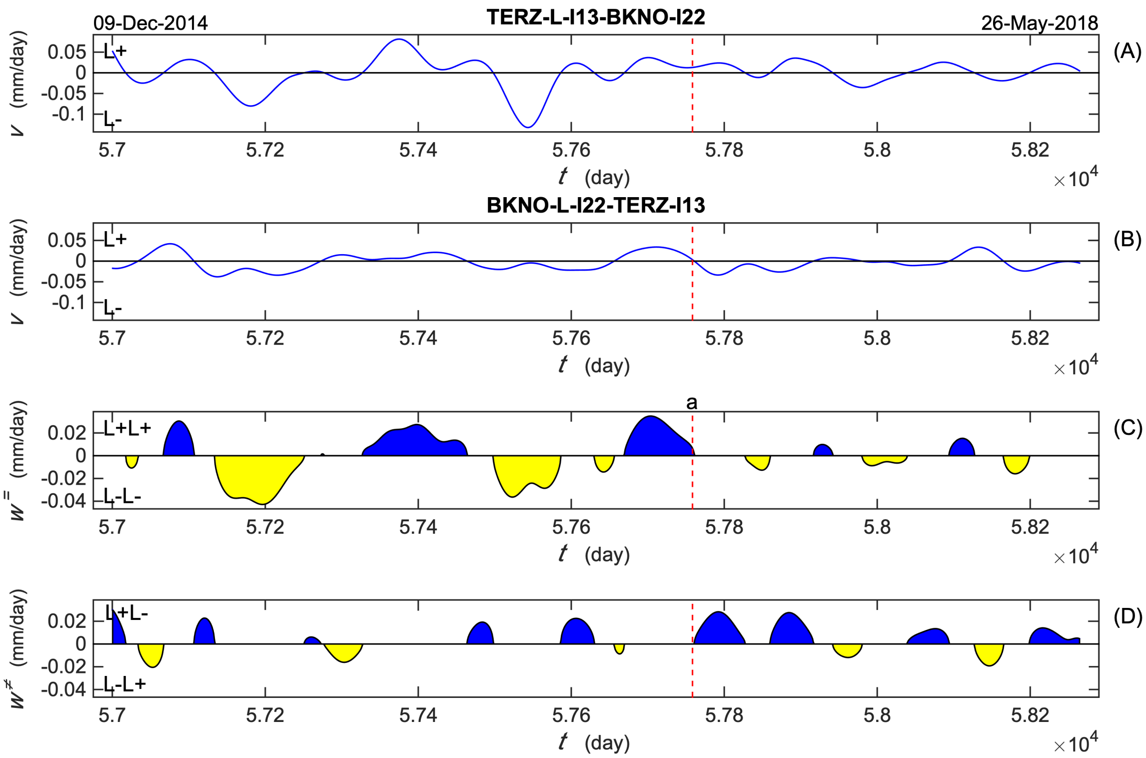

Fig. 9 Co-velocities comparison for longitudinal components at TERZ and BKNO. The vertical dotted line indicates $t = 57758$.

Snapshots

The fourth interpretation tool considers together all velocities, shown as vectors, and their vertical and horizontal components, through what we call snapshots. A snapshot is a record of the velocity status of the network at a given time; consisting of both a listing of the measured velocity components (the Z or Up component is halved to correct for the free-surface effect) and the resulting velocity vector and its azimuth and elevation, and a 3-D figure that can be rotated to show how velocities were oriented at that particular time. Figure 10 (A) shows the three velocity components at all stations, and the vertical dashed line indicates the time $t = 57769$ of a snapshot. At this time velocities were as described in Table 2 and illustrated in Fig. 10 (B); stations ONPI, OSVE, and VOLL were not recording at the time.

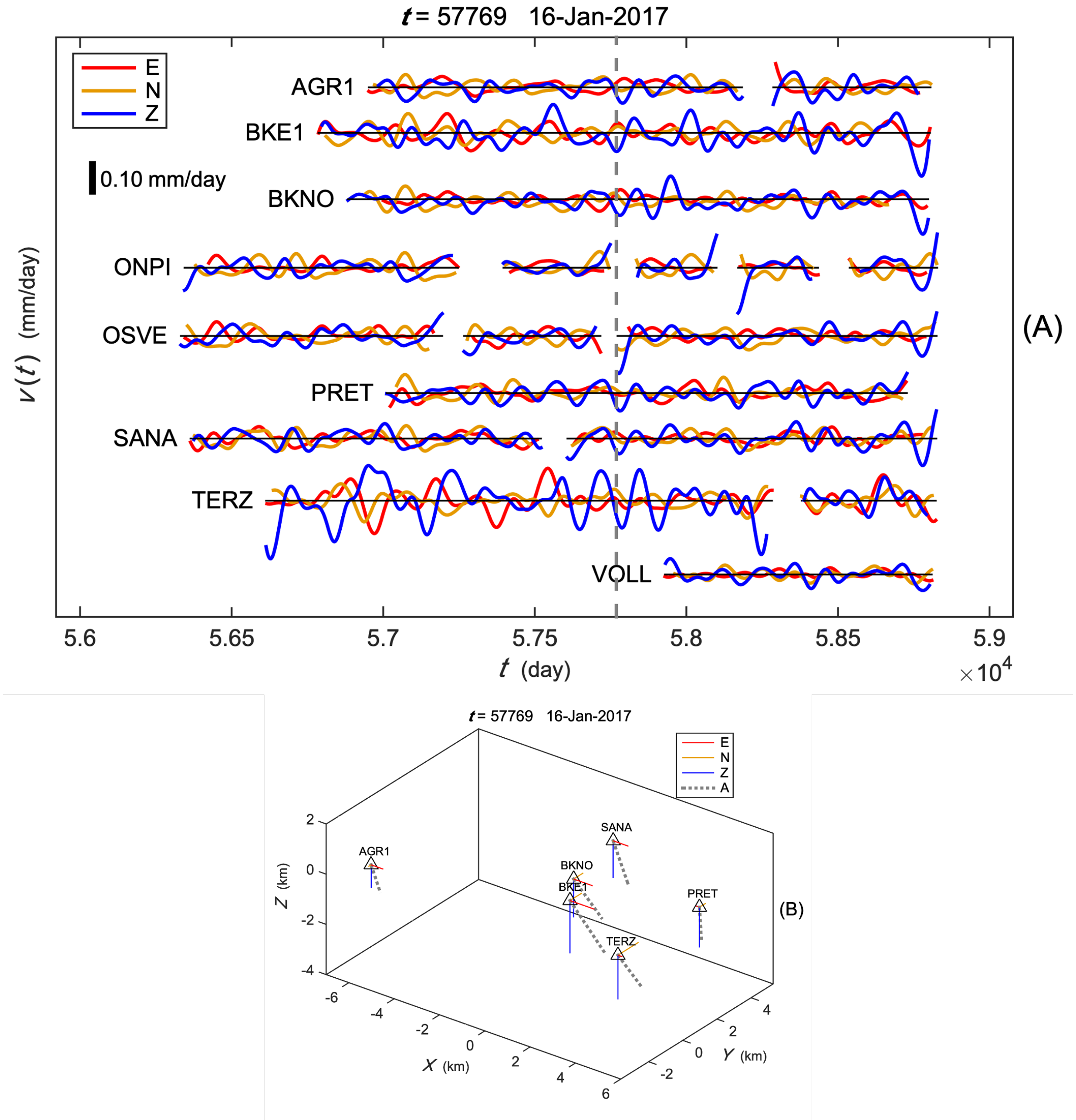

Fig. 10 Display of all the velocity signals for the latter segments of the recorded series (A), and a snapshot of velocities at all stations for time $t = 57769$ (B).

Table 2 Snapshot of velocities at time $t = 57769$, illustrated in Fig.10 (B)

$t = 57769$ (16 Jan., 2017)				
Station	V_E mm/day	V_N mm/day	V_Z mm/day	$\lvert V \rvert$ mm/day

AGR1	0.0171	-0.0046	-0.0298	0.0347
BKE1	0.0353	0.0227	-0.0695	0.0812
BKNO	0.0274	0.0181	-0.0504	0.0601
PRET	-0.0055	0.0113	-0.0528	0.0543
SANA	0.0217	-0.0004	-0.0488	0.0534
TERZ	0.0058	0.0395	-0.0580	0.0704

Cartoons

In order to interpret the velocity observations, it would be useful to have a realistic model of the volcano and the source, but the source and its location are not known and the volcanic structures are usually quite complicated and poorly known. Thus, to help interpret the observations we take recourse to model so simplistic that we call it a cartoon, consisting of a radially symmetric source in a homogeneous medium; velocity amplitudes decrease with distance as the square root.

In such a model, an expanding source would cause stations on each side to register velocities pointing away from the source, so that stations located on different sides of the source would both be moving up but in opposite horizontal directions, while stations on the same side would both be moving up and in roughly the same horizontal direction. For a contracting source, stations on opposite sides of it would have velocities pointing towards the source. Of course, more complicated source behaviors can give rise to motions that are more difficult to interpret but knowing the relative motion directions might also be helpful.

Different source positions, contracting or expanding, can be proposed to see which one results in velocities that resemble the observed ones.

Figure 11 is a cartoon showing how the velocities would be for a source located at (5.4645, 2.0763, -6.2332) (the source found below for an approximate location at time $t = 57769$).

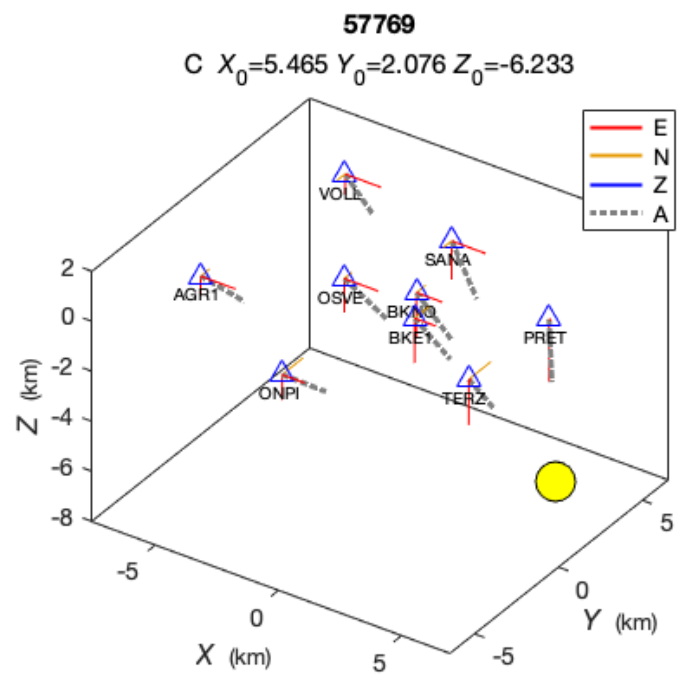

Fig. 11 Cartoon showing how velocities would be for a contracting source represented by a yellow circle. Velocity components are color-coded and the total velocity amplitude is represented as a thick, gray dotted line, with lengths proportional to the velocity amplitudes.

The total velocity vectors are shown in Fig. 11 as dashed thick lines associated with each station with lengths proportional to $|V|$, and their orientation points towards the source.

Snapshots and Approximate Locations

Snapshots very seldom show a simple pattern that could be easily interpreted using cartoons, and many feature apparent contradictions that could be due to a complex distribution of the source(s) or to site effects, but could also be caused by noise. Noise is unavoidable and can be an important factor when velocities are small, in which case even a little noise can significantly modify the velocity vector direction and can even change the polarity of a velocity component.

In rare instances snapshots show velocity vectors that agree reasonably well among them, and in these cases a very rough, approximate location can be tried. A way to obtain an approximate location is by propagating backwards the velocity vectors. For each pair of stations, the horizontal velocity components are propagated backwards to obtain their intersection in the X-Y plane, then the vectorial total velocity is propagated backwards from each station until it reaches the point below the horizontal intersection, usually at a different depth for each station. This procedure results in having generally two source solutions for each pair of stations, for a total $N_s = N(N-1)$ solutions, where N is the number of stations.

This method works perfectly for synthetic (cartoon) data without noise, but if noise is added to the synthetic data the solutions start to spread. For normal noise with a standard deviation as small as 0.05 times the largest velocity, some solutions can differ by large amounts.

Due to the above-mentioned discrepancies, solutions always differ for real snapshot data, but sometimes an acceptable, if approximate, location can be obtained by: first discarding stations featuring vertical velocities with different signs from those of the majority (if there is no majority or the number of positive vertical velocities is very close to that of negative ones, there is no reasonable solution). Next, assigning to each station a weight proportional to the total amplitude, and to each solution a weight corresponding to the product of the weights of the two stations involved. Finally, iteratively finding the weighted mean for each component of the source position, calculating the standard deviation of the solutions from that mean, and discarding outliers differing from the weighted mean by more than a given number of standard deviations or chosen by eye, until a satisfactory solution is found or until it is clear that there are no satisfactory solutions.

Figure 12 shows one location obtained from the velocities at the time indicated by a vertical dotted line in Fig. 10. From the 30 original solutions giving the raw source coordinates (with uncertainties corresponding to one standard deviation S) $X_0 = -6.879 \pm 30.308$ km, $Y_0 = -5.780 \pm 19.296$ km, and $Z_0 = -30.703 \pm 52.528$ km, after 3 eliminations of outliers with positions >3S and 3 for >2.5S and manual elimination of 3 solutions, from the remaining 13 solutions we get a final approximate location $X_0 = -5.465 \pm 0.604$ km, $Y_0 = 2.076 \pm 1.303$ km, and $Z_0 = -6.233 \pm 2.522$ km. The velocities resulting in this location can be compared with the cartoon velocities for the same source location in Fig. 11.

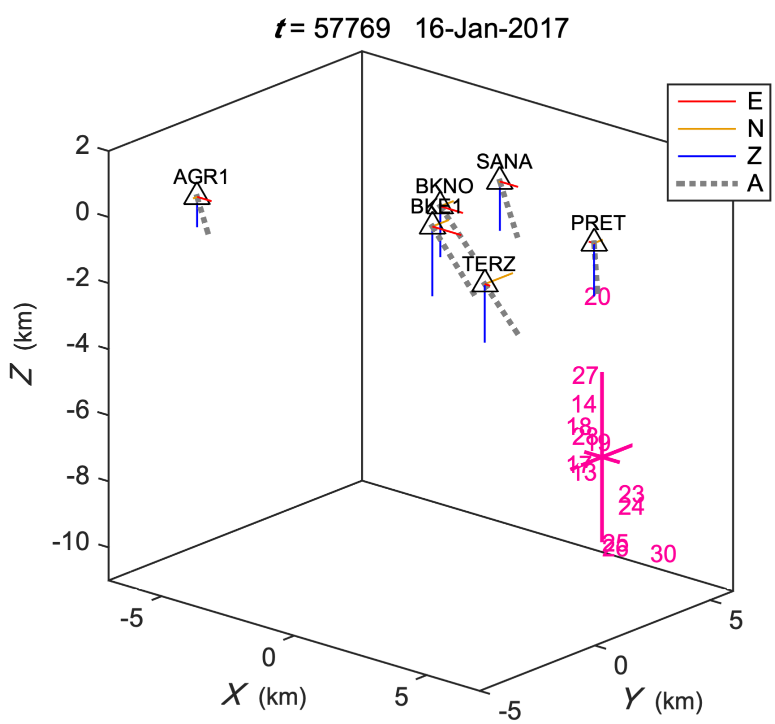

Fig. 12 Example of approximate location from a snapshot of observed velocities. The numbers indicate the location of the solutions; there are two numbers for each pair of stations, assigned alphabetically. The weighted mean solution is at the intersection of the three magenta lines whose lengths correspond to the standard deviations in each direction.

Discussion and conclusions

As mentioned above, using velocities has several advantages over using displacements, the main one is having a definite reference zero level, which lets velocities be compared and be treated as vectors. Since velocities are proportional to the instantaneous displacements (Eq. 1), any conclusions derived from velocities can be readily applied to displacements by going back to the displacement time series and taking into account the times or features of interest determined from the velocities.

However, working with velocities has some disadvantages. Since the derivative is a high-pass filter, the series require stronger low-pass filtering to give a useful picture of medium- and long-period features of the volcanic deformations. Also, velocities are sensitive to high-frequency noise that can distort information, particularly when velocities are small; yet small velocities can yield important information, a station moving towards or away from a source located directly East or West of it, should have null, or very small, N-S velocity components.

The approach and the tools we present here, while not contributing additional information from that contained in the position time series, can make some behaviors of the volcanic sources easier to appreciate, and comparisons easier to understand and evaluate.

We hope that the material presented in this paper, will be useful to scientists working with cGPS/GNSS data from volcanoes, and may help them to make contributions to the better understanding of the volcanic processes.

Acknowledgments

We are grateful to Prospero De Martino, Mario Dolce, Giuseppe Brandi, Giovanni, Scarpato, and Umberto Tammaro for generously sharing their data with the scientific community. L. A.-B. was supported by the CONAHCYT *Investigadoras e Investigadores por México* program, project 7095.

Statements and Declarations

Competing Interests

The authors declare that there are no conflicts of interest or competing interests.

Authorship contribution statement

F. A. Nava: Conceptualization, Program code, Data analysis, Writing – First draft, review of subsequent drafts. L. Ávila-Barrientos: Data analysis, Writing – contributions to and review of all drafts, editing. C. E. Reinoza: Data analysis, Writing – contributions to and review of all drafts, editing.

Funding

This study had no external funding.

Data availability

The data are available in De Martino et al. (2021)

References

Ávila-Barrientos L, Cabral-Cano E, Nava FAP, Reinoza CE, Salazar-Tlaczani L, Fernández-Torres E (2021) Surface deformation of Ceboruco volcano, Nayarit, Mexico. Journal of Volcanology and Geothermal Research, Vol. 418. https://doi.org/10.1016/j.jvolgeores.2021.107338

Bartel BA, Hamburger MW, Meertens CM, Lowry A, Corpuz E (2003) Dynamics of active magmatic and hydrothermal systems at Taal Volcano, Philippines, from continuous GPS measurements. Journal of Geophysical Research, Vol. 108, No. B10, 2475, doi:10.1029/2002JB002194

Cabral-Cano E, Correa-Mora F, Meertens C (2008) Deformation of Popocatépetl volcano using GPS: Regional geodynamic context and constrains on its magma chamber. Journal of volcanology and geothermal research. 170, 24-34.

Chaussard E, Amelung F, Aoki Y (2013) Characterization of open and closed volcanic systems in Indonesia and Mexico using InSAR time series. Journal of Geophysical Research: Solid Earth, Vol. 118, 3957-3969. doi:10.1002/jgrb.50288

De Martino P, Dolce M, Brandi G, Scarpato G, Tammaro U (2021) The The Ground Deformation History of the Neapolitan Volcanic Area (Campi Flegrei Caldera, Somma–Vesuvius Volcano, and Ischia Island) from 20 Years of Continuous GPS Observations (2000–2019). Remote Sens.2021,13,2725. https:// doi.org/10.3390/rs13142725

Dixon HT, Mao A, Bursik M, Heflin M, Langbein J, Stein R, Webb F (1997) Continuous monitoring of surface deformation at Long Valley Caldera, California, with GPS. Journal of Geophysical Research, Vol. 102, No. B6, pp. 12,017-12,034.

Fournier T, Freymueller J, Cervelli P (2009) Tracking magma volume recovery at Okmok volcano using GPS and an unscented Kalman filter. Journal of Geophysical Research. Vol. 114, B02405. doi:10.1029/2008JB005837

Ghosh B, Motagh M, Haghshenas MH, Stefanova MV, Walter TR, Maghsudi S (2021) Automatic Detection of Volcanic Unrest Using Blind Source Separation With a Minimum Spanning Tree Based Stability Analysis. Ieee Journal of Selected Topics in Applied Earth Observations and Remote Sensing, vol. 14.

Hamming R (1977) Digital filters. Prentice Hall.

Hotta K, Iguchi M, Ohkura T, Hendrasto M, Gunawan H, Rosadi U, Kriswati E (2019) Magma intrusion and effusion at Sinabung volcano, Indonesia, from 2013 to 2016, as revealed by continuous GPS observation. Journal of Volcanology and Geothermal Research, 382, 173-183.

Janssen V (2007) Volcano deformation monitoring using GPS, Journal of Spatial Science, 52:1, 41-54, DOI: 10.1080/14498596.2007.9635099

Janssen V, Roberts C, Rizos C, Abidin HZ (2002) Low-cost GPS-based volcano deformation monitoring at Mt. Papandayan, Indonesia, Journal of Volcanology and Geothermal Research, vol. 115, no. 1-2, pp. 139-151.

Larson KM, Poland M, Miklius A (2010) Volcano monitoring using GPS: Developing data analysis strategies based on the June 2007 Kilauea Volcano intrusion and eruption. Journal of Geophysical Research, Vol. 115, doi:10.1029/2009JB007022.

Lee S-W, Yun S-H, Kim DH, Lee D, Lee YJ, Schutz BE (2015) Real-time volcano monitoring using GNSS single-frequency receivers, Journal of Geophysical Research. Solid Earth, 120, 8551–8569, doi:10.1002/2014JB011648

Lowry AR, Hamburger MW, Meertens CM, Ramos EG (2001) GPS monitoring of crustal deformation at Taal Volcano, Philippines. Journal of Volcanology and Geothermal Research, 105, pp. 35-47.

Mann D, Freymueller J, Lu Z (2002) Deformation associated with the 1997 eruption of Okmok volcano, Alaska. Journal of Geophysical Research. Vol. 107, No. B4, 2072.

Miyagi Y, Freymueller JT, Kimata F, Sato T, Mann D (2004) Surface deformation caused by shallow magmatic activity at Okmok volcano, Alaska, detected by GPS campaigns 2000-2002. Earth Planets Space, 56, e29-e32.

Mogi K (1958) Relations between the eruptions of various volcanoes and the deformations of the ground surfaces around them. Bulletin of the Earthquake Research Institute. Vol. 36, pp. 99-134.

Moran SC, Freymueller JT, LaHusen RG, McGee KA, Poland MP, Power JA, Schmidt DA, Schneider DJ, Stephens G, Werner CA, White RA (2008) Instrumentation recommendations for volcano monitoring at U.S. volcanoes under the National Volcano Early Warning System: U.S. Geological Survey Scientific Investigations Report 2008-5114, 47 p.

Nishimura T, Ozawa S, Murakami M, Sagiya T, Tada T, Kaidzu M, Ukawa M (2001) Crustal deformation caused by magma migration in the northern Izu Islands, Japan. Geophysical Research Letters. Vol. 28, No. 19, Pages 3745-3748.

Salzer JT, Nikkhoo M, Walter TR, Sudhaus H, Reyes-Dávila G, Bretón M, Arámbula R (2014) Satellite radar data reveal short-term pre-explosive displacements and a complex conduit system at Volcán de Colima, Mexico. Frontiers in Earth Sciences, 2, 12. doi: 10.3389/feart.2014.00012

Savage MK, Ohminato T, Aoki Y, Tsuji H, Greve SM (2010) Stress magnitude and its temporal variation at Mt. Asama Volcano, Japan, from seismic anisotropy and GPS. Earth and Planetary Sciences Letters, 290, pp. 403 – 414.

Tilling RI (2008) The critical role of volcano monitoring in risk reduction. Advances in Geosciences, 14, 3-11.